

Space-Time Picture of Fragmentation in PYTHIA/JETSET for HERMES and RHIC

K. Gallmeister*, T. Falter

Institut für Theoretische Physik, Universität Giessen, Germany

Abstract

We examine the space-time evolution of (pre-)hadron production within the Lund string fragmentation model. The complete four-dimensional information of the string breaking vertices and the meeting points of the prehadron constituents are extracted for each single event in Monte Carlo simulations using the JETSET-part of PYTHIA. We discuss the implication on the deep inelastic lepton scattering experiments at HERMES as well as on observables in ultra-relativistic heavy ion collisions at RHIC, using PYTHIA also for modeling the hard part of the interaction.

Key words: hadron formation, Lund model, deep inelastic scattering, electroproduction, hadron induced high-energy interactions, meson production
PACS: 12.38.Lg, 13.60.-r, 13.85.-t, 25.75.-q, 25.30.c

The fragmentation of high energy quarks into color-neutral hadrons is a subject of high current interest. So far one cannot describe the complete space-time picture of this process within QCD as the underlying theory. The reason is that the formation of hadrons involves momentum scales of only a few hundred MeV which rules out a purely perturbative approach. Furthermore, the complexity of the fragmentation process goes far beyond what can be addressed by current non-perturbative lattice-QCD calculations.

Estimates based on perturbative QCD (1) suggest, that the formation time of a hadron, i.e. the time needed to build up the hadronic wave function, is of the order of 1 fm/c in the hadron's restframe. At large enough energies these eigentimes correspond to formation lengths in the lab frame which are comparable with nuclear dimensions. If the fragmentation process is modified by the surrounding nuclear medium, an experimental comparison of high

* Corresponding author.

Email address: Kai.Gallmeister@theo.physik.uni-giessen.de
(K. Gallmeister).

energy hadron production on various nuclear targets with different radii can give insight into the space-time picture of hadronization. With that respect the nucleus can be considered as a micro-laboratory for fragmentation studies.

In the recent past the HERMES collaboration at DESY has carried out an extensive experimental study of hadron attenuation (2) in deep inelastic lepton-nucleus scattering (DIS). Depending on the evolution of the fragmentation process in space-time the observed signals might either be dominated by (pre-)hadronic final state interactions (FSI) (3; 4; 5; 6) or by a partonic energy loss prior to fragmentation (7). A detailed investigation of this subject is also essential for the interpretation of ongoing experiments at hadron colliders like RHIC or the future LHC which among other topics intend to find experimental evidence for a new QCD-phase, the Quark-Gluon-Plasma (QGP). (Pre-)hadronic FSI could contribute to the suppression of high- p_{\perp} hadrons and thereby modify jet-like signatures that are still considered clean proofs for the creation of a deconfined QGP phase (8; 9).

The Monte Carlo event generator PYTHIA (10) has become one of the standard tools to perform calculations in the kinematic regimes that we have just mentioned (6; 8; 11). The fragmentation in PYTHIA is based on the Lund string model (12). In former versions of PYTHIA the routines handling the string fragmentation were bundled in a separate package called JETSET. We keep this (old fashioned) nomenclature throughout this work in order to distinguish between the part of the event generator that creates the hadronic strings (e.g. PYTHIA, FRITIOF (13) etc.) and the part that is responsible for the string fragmentation (JETSET). A detailed description of the underlying model of JETSET can be found in Ref. (14). In JETSET the eigentimes of the string breaking vertices are determined during the fragmentation. However, the real essential information, namely the four-dimensional space-time coordinates of the string breaking, is not reported.

In this work we present a detailed quantitative analysis of the four-dimensional space-time picture of hadron production with PYTHIA/JETSET in soft and hard interactions at HERMES and RHIC energies. We show for the first time the exact spatiotemporal distribution of (pre-)hadron production and formation points in realistic ep and pp collisions at HERMES and RHIC. Thereby we take into account complications like resolved photon interactions, gluon radiation, primordial transverse momenta of quarks, transverse momentum generation in the string fragmentation, cluster decay, finite mass effects, quark flavor dependence, diquark production, etc. Although our results should not be overstressed since one applies a semi-classical picture to a quantum mechanical problem, our approach makes it possible to assign the four-dimensional production and formation point to each single hadron in each single scattering event. This sets the foundation for consistently using the PYTHIA model for both the determination of hadron momentum spectra – where the model has

been successfully tested – and the description of the space-time evolution of hadron production. Both information can then be used in a consistent way as input for future transport simulations such as the BUU (5) or the HSD model (9) to describe nuclear reactions at HERMES and RHIC energies and to determine the contribution of the (pre-)hadronic FSI to the experimentally observed hadron attenuation. Since the application of our findings is not restricted to one single nuclear reaction model, we exclude any specific modeling of the (pre-)hadronic FSI at this stage and merely concentrate on the space-time evolution of the (vacuum) fragmentation process in this work.

Although we use PYTHIA to produce the initial string configurations we emphasize, that this is no restriction concerning the extraction of the four-dimensional fragmentation coordinates, since the fragmentation routines are independent of the string-building routines. It is therefore “ab initio” straightforward, to transfer our method to other event generators, supposed they use JETSET for fragmentation.

In principle, one could distinguish two classes of ‘strings’: strings that are made up of a quark and an antiquark only and those with additional (hard) gluons located between the string ends as transversal excitations. (We will not touch strings build up entirely of gluons in this work. Here the mechanisms at work are far beyond being transparent. On the other hand, they are very rarely produced at the HERMES energies and also play a minor role interpreting current RHIC findings.) However, this distinction is purely artificial, because the latter reduces to the first case in the limit of vanishing transverse gluon momenta (14). We point out that PYTHIA also allows for diquarks at the string ends as well as the creation of diquark-antidiquark pairs in the string fragmentation. This possibility is accounted for in our computer code but omitted for the sake of better readability in the following text.

JETSET includes two different hadronization methods for an initial partonic system: ‘string fragmentation’ and ‘cluster decay’ where only the first one is based on the actual Lund fragmentation model. The latter method is constructed in such a way that it reproduces the rapidity distributions of the Lund fragmentation. Which of these two methods is used for hadronization depends mainly on the invariant mass of the decaying system.

We begin with a review of the fragmentation of an one-dimensional string, i.e. a string that consists of a quark and an antiquark string end and no gluonic excitation. Note that, most authors that discuss ‘string fragmentation’ restrict themselves to this one type of all possibilities. It can easily be illustrated and analytic expressions can be found, e.g. in Refs. (3; 12; 15). We thus explain the necessary formalism by means of this example (cf. Fig. 1). We stress, that all momenta and coordinates in Fig. 1 are four-vectors and not light-cone variables.

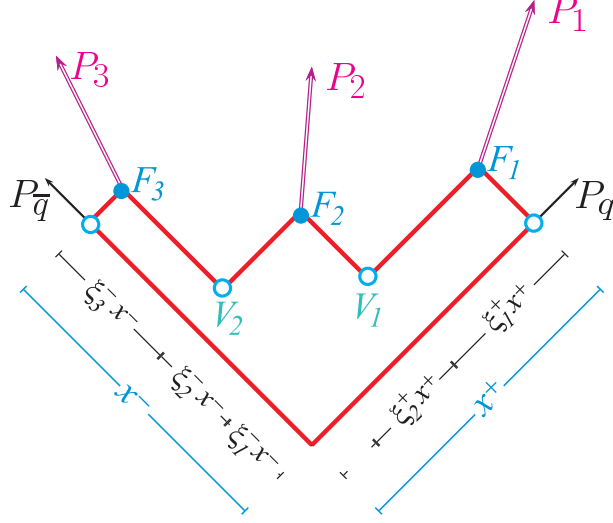


Fig. 1. A sketch of the fragmentation of an one-dimensional $q\bar{q}$ -String (in the rest frame of the string). The P_x denote momenta, while V_i indicate string breaking vertices (production points) and the F_i the yoyo-formation points of the hadrons. While in principle all vectors are four-dimensional, in this sketch the horizontal axis is the x -axis and the vertical coordinate is the time t . Please note: not lightcone formalism, but four-vectors.

In the following, we set the string tension to $\kappa = 1 \text{ GeV/fm}$. This allows us to omit κ in all formulae and to identify momentum vectors with space-time coordinates, i.e.

$$P_q = x^+, \quad P_{\bar{q}} = x^- \quad (1)$$

where P_q ($P_{\bar{q}}$) and x^+ (x^-) denote the initial four-momentum and turning-point of the (anti-)quark respectively. The four-momenta P_i of the final hadrons are given by

$$P_i = \xi_i^+ x^+ + \xi_i^- x^- \quad (2)$$

with the constraints $0 \leq \xi_i^\pm \leq 1$ and $\sum \xi_i^\pm = 1$. For each hadron ξ_i^+ and ξ_i^- are obviously related via the (transverse) mass m_i of the produced hadron. In Eq. (2) we have neglected any transverse momenta created in the string breakings for simplicity. The following formulae are not affected by this simplification. The space-time positions of the string breakings (production points) are

$$V_i = \chi_i^+ x^+ + \chi_i^- x^- \quad (3)$$

with $\chi_i^+ = 1 - \sum_{j=1}^i \xi_j^+$, $\chi_i^- = 0 + \sum_{j=1}^i \xi_j^-$ and the points where the world-lines of the constituents of hadron i meet for the first time – usually called

the 'yoyo-formation point' of hadron i – are given as

$$F_i = \chi_i^+ x^+ + \chi_{i+1}^- x^- . \quad (4)$$

One should keep in mind, that the latter only makes sense if one neglects any transverse momentum of the $\bar{q}q$ -pairs created at the string breaking vertices. In general, a quark from one vertex – having some transverse momentum – does not cross the trajectory of an antiquark that stems from another vertex and has some other transverse momentum. We point out that the yoyo-formation points do not necessarily correspond to the real formation points of the hadron, i.e. the space-time point where the full hadronic wavefunction has built up.

Obviously, both the production and formation points in space-time can be reconstructed from the initial quark and antiquark momenta P_q and $P_{\bar{q}}$ if one extracts the complete set of ξ_i^\pm from JETSET. (Please recall: All the transversal momentum components are only necessary to reconstruct the hadron momenta, not the fragmentation points.)

We now concentrate on the implementation of the string fragmentation in JETSET. Like all other Lund-implementations it suffers from the fact that in the derivation of the fragmentation function one assumes that the decaying string has infinite mass (14). If one starts on one side of the string (e.g. the quark string end) and continues the fragmentation to the other side (i.e. the antiquark string end), one will run into the problem of finding a solution for the last hadron that both conserves energy and momentum and fulfills the mass-shell condition for the hadron. In order to avoid this problem, JETSET randomly performs fragmentations at one or the other side of the decaying string, until the invariant mass of the remaining string system (somewhere in the middle of the string) falls below some threshold value. Then JETSET switches to a mode in which the parameters of the two final hadrons are chosen simultaneously in such a way that energy and momentum are conserved and that the rapidity distribution of the hadrons looks like in the original Lund fragmentation process (10; 16). This method is very similar to the one used for the 'cluster decay' discussed below.

So far, the production and formation points could be determined by Eqs. (3) and (4) respectively. However, strings may have transverse excitations, which are represented by additional gluons between the string ends. These gluons impose some transverse momentum on the string and lead to a complex movement of the string in space-time which is known as the 'dance of the butterfly' (12).

The additional gluons split the string into separate regions. For a configuration that consists of a quark, $n - 2$ gluons and an antiquark with related four-momenta $q(p_1)$, $g(p_2)$, \dots , $g(p_{n-1})$, $\bar{q}(p_n)$ the initial string contains $n - 1$

pieces. In four-momentum space the i -th string piece is spanned by the two four-momenta $p_{(i)}^+$ and $p_{(i)}^-$ where we have defined $p_{(1)}^+ = p_1$, $p_{(1)}^- = p_2/2$, $p_{(2)}^+ = p_2/2$, $p_{(2)}^- = p_3/2$, \dots , $p_{(n-1)}^+ = p_{n-1}/2$, $p_{(n-1)}^- = p_n$ in analogy to the simple $q\bar{q}$ -string (Eq. (1)). The factors $1/2$ arise because the gluons share their energy between the two adjacent string pieces.

Due to the complex movement of the string new regions appear as time goes by. Each region can be thought of being spanned by one $p_{(j)}^+$ and another $p_{(k)}^-$ four-vector with j and k not necessarily adjacent. It is straightforward, but tedious and not illuminating, to extend Eqs. (2) and (4) to the case of multiple string pieces (14). Therefore we only comment on the major complications: Since now the string(-part) ends have initial “transversal” momentum components, transverse momenta of the quarks originating from the string breakings must be considered explicitly. Hadrons built up from partons that are created in different string regions cause severe problems in the string fragmentation. Simplifications that are made in the JETSET code to cure this problems result in faulty four-dimensional coordinates of the fragmentation points (14).

As pointed out not every string configuration in JETSET decays according to the Lund fragmentation scheme. Depending on the invariant mass of the system it may also fragment according to a cluster decay algorithm where the final state may only consist of one or two hadrons. In case of the decay into one hadron, the strings’s four-momentum is mapped onto the four-momentum of the final hadron. Since the hadron mass is more or less fixed, left over components are transferred to a nearby string in form of a gluon with the corresponding four-momentum. If the cluster decays into two hadrons, the same algorithm as for the two last hadrons in the usual string fragmentation is applied. For details we refer the reader to Ref. (10) and references therein. Production vertices of hadrons stemming from cluster decays are assumed to be at the interaction point. In case of a cluster decay into two hadrons, the four-dimensional information of the second, i.e. the “middle” quark-antiquark production point, is reconstructed from energy-momentum constraints in analogy to Eq. (3). Also the formation points are determined from the four-momenta of the hadrons in analogy to Eq. (4).

Since JETSET does not report any space-time vectors concerning the fragmentation progress, this has to be done manually. We enhanced the corresponding routines to report some informations such as the ξ_i^\pm , which enable us to calculate each string breaking point and all meeting points in four dimensions. Please recall, that this is all the information we need. We have checked, that the proper times reconstructed from these values match those used in the fragmentation process.

As an example we consider the fragmentation of a $qg\bar{q}$ -string with JETSET. For simplification purposes we switched off transverse momentum production

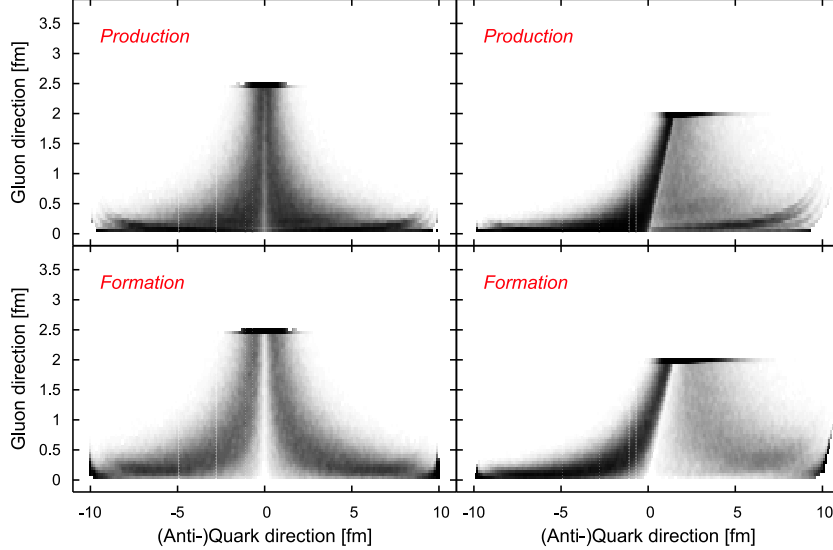


Fig. 2. *Distribution of production (upper panel) and formation points (lower panel) for the example $P_{q,\bar{q}} = (\pm 10, 0)$ GeV, $P_g = (0, 5)$ GeV (left) and $P_g = (3, 4)$ GeV (right). Dark regions refer to larger decay and formation probabilities.*

at the string breaking vertices. On the left hand side of Fig. 2 we show the spatial distributions of the string breakings, i.e. production points, and the yoyo-formation points for a system where the quark and antiquark momenta (± 10 GeV) are along the x -axis (with opposite directions) and the gluon moves perpendicular to them into the y -direction (5 GeV). The spatial boundaries of the production points are set by the initial (anti-)quark and gluon momenta. Since the gluon loses energy to both the adjacent string pieces the production points have transverse coordinates $y \leq 2.5$ fm. As one might have expected, the yoyo-formation points are slightly shifted outwards compared to the production points. Taking the same parameters, but slightly tilting the gluon momentum out of the transversal direction, the spatial distributions change according to the right hand side of Fig. 2. Please note however, that these are more or less pathological examples, since in real event simulations (some hard scattering with initial and final state radiation) string regions with invariant masses as large as chosen here are quite rare.

The sharp structures, best seen in the distribution of the production points for the tilted gluon (Fig. 2, right top), are due to mass constraints and only visible, if one neglects transversal momenta, as done in this example: Structures caused by different hadron masses m are smeared if one has to switch to the transverse mass m_{\perp} . We point out, that we have excluded production and formation points, which are due to a faulty reconstruction caused by the abovementioned simplifications in the JETSET code. These would give rise to spurious points at transversal components larger than what is allowed by the gluon component and contribute with less than two percent to the total yield.

In both cases one clearly identifies a new string region as the horizontal dis-

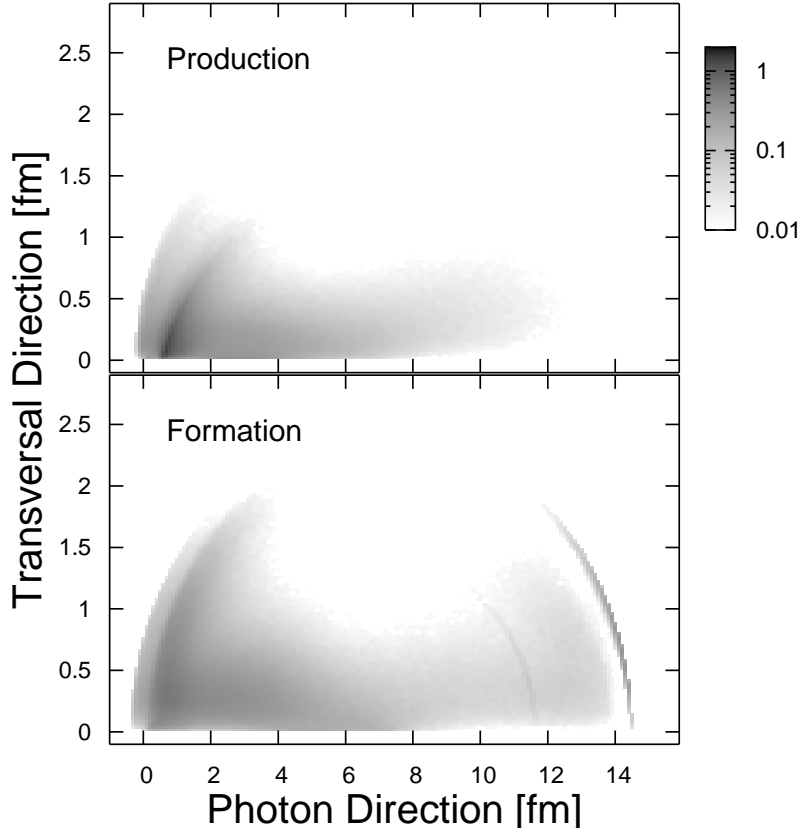


Fig. 3. *Production (top) and formation (bottom) points for a typical Hermes event: ($\nu = 14 \text{ GeV}$, $Q^2 = 2.5 \text{ GeV}^2$). The target nucleon is located at the origin, the virtual photon is coming in from the left. Labels in the plots correspond to explanations in the text.*

tribution displaced from the x -axis. This region appears in the time-evolution of the string after the gluon has lost all of its momentum to the string.

We now apply our method of extracting four-dimensional vertices to two practical examples. The first is an electron (virtual gamma) induced reaction on a nucleon at HERMES energies and the second one is a pp -collision at RHIC energies.

The experimental data on γ^*p and γ^*A reactions at HERMES imply some complicated kinematic cuts, e.g. in the ν - Q^2 -plane where ν denotes the photon's energy and Q^2 its virtuality. In this study we will neglect this complication and simply replace the whole averaging over a multi dimensional parameter space by using some mean values. Since the underlying physical processes vary drastically (e.g. importance of resolved photon-nucleon interactions) within the full experimentally accessible kinematical region, our example is not representative for *all* possible HERMES events. In Fig. 3 we show the spatial distribution of production and formation points for a γ^*p -reaction at $\langle \nu \rangle = 14 \text{ GeV}$ and $\langle Q^2 \rangle = 2.5 \text{ GeV}^2$. This corresponds to an invariant mass $\langle W \rangle = 5 \text{ GeV}$ of the photon-nucleon system. The photon is coming in from the

left and strikes a nucleon which is located at the origin. While PYTHIA describes all spectra of non-charmed hadrons at HERMES energies astonishingly well (5; 6; 11), its ability to describe charm production has never been tested in this kinematic regime. We therefore exclude all charmed hadrons from our analysis. Note that both production and formation points lie mainly inside a radius of ~ 6 fm around the interaction point. If one compares these values with a typical diameter of a complex nucleus one might expect strong (pre-)hadronic FSI after the (production) formation time in case of photonuclear reactions.

In contrast to common belief the DIS does not simply lead to a one-dimensional string configuration. Instead of that, the distributions in Fig. 3 show some (elliptical) structures which are again due to non vanishing mass terms and need some more detailed explanations: Due to kinematics all production and formations points lie within circles of radius $W/2$ in the cm-frame of the photon-nucleon system. By boosting to the lab frame one obtains the observed ellipses with maximum transverse dimension $W/2$ and extremal longitudinal values of $x_z^- \simeq -0.4$ fm and $x_z^+ \simeq 14.5$ fm.

The transversal distribution of the vertices is caused by two mechanisms. The first one is the transverse momentum p_\perp generated in the string breakings that leads to a small transverse spread which is best seen at longitudinal distances around 7 fm. The by far more important effect, however, stems from the intrinsic transverse momentum k_\perp of the nucleon constituents. This can easily be understood by considering the simple scenario, where the virtual photon gets absorbed by a single quark inside the proton. In that case a single string is spanned between a diquark at the origin and the struck quark. Without intrinsic momenta, such a string would simply expand along the initial photon direction. The intrinsic k_\perp rotates the direction of the string (without changing its invariant mass) and leads to the transversal distribution of production and formation points. (We used the default value $\langle k_\perp^2 \rangle = 1 \text{ GeV}^2$ of PYTHIA in our simulations.)

The yoyo-formation point of the first-rank hadron, i.e. the hadron labeled '1' in Fig. 1, is given by $x^+ + \xi_1^- x^-$. In the case of one single quark-diquark string its longitudinal coordinate in the lab frame is therefore confined to the narrow region between 14.1 fm and 14.5 fm if one neglects all transverse momenta. Correspondingly, the formation point of the highest-rank hadron, i.e. the hadron labeled '3' in Fig. 1, is given by $x^- + \xi_n^+ x^+$ and, hence, its longitudinal coordinate lies between -0.4 fm and 14.1 fm. The finite invariant mass W of the string gives rise to a lower boundary ($\xi^\pm \geq (m_h/W)^2$) for the possible ξ -values. This lower limit leads to the two distinct branches that are visible in Fig. 3: While the lower limit is negligible for pions, it becomes important for the heavier mesons and baryons; as a consequence the latter have formation points with larger (here: positive) longitudinal component. A

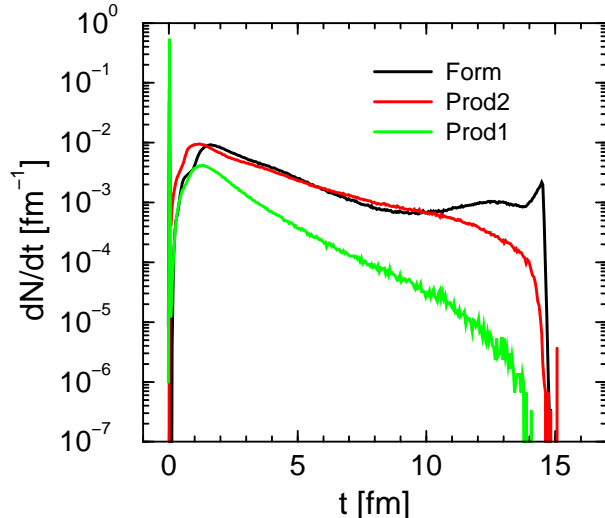


Fig. 4. Distributions of the production times t_1 , t_2 and the formation time t_F for a virtual γ^*p event. The kinematics are the same as for Fig. 3 ($\nu = 14 \text{ GeV}$, $Q^2 = 2.5 \text{ GeV}^2$).

similar (but more involved) mechanism is at work for the production points and leads to the strong (dark) band at low longitudinal positions.

The importance of the production points for hadron attenuation in nuclear reactions has been extensively discussed in Refs. (3; 4; 5; 6; 9). The constituents of a hadron that is formed at point F_i in Fig. 1 are produced at the string-breaking vertices V_i and V_{i-1} . We denote the larger of the two production times t_2 and the smaller one t_1 . At the later production point, i.e. at time t_2 , the string splits into a color neutral object (prehadron) – which has the four-momentum of the final hadron – and a remainder string. The final state interactions of this prehadron with the nuclear environment modify the spectrum of the ultimately detected hadrons but do not influence the actual string fragmentation process. Fig. 4 shows the distributions of the production times t_1 and t_2 of the first and second hadron constituents as well as the yoyo-formation times t_F . The structures in the time distributions simply reflect the complex features that already showed up in Fig. 3. The presented distributions might be used as input for various attenuation studies such as the recent prehadron absorption model of Ref. (17).

In Fig. 5 we show the average production times $\langle t_1 \rangle$ and $\langle t_2 \rangle$ as well as the average formation time $\langle t_F \rangle$ as function of the fractional hadron energy $z_h = E_h/\nu$. One clearly sees that the hadron formation times increase with energy whereas the production times of prehadrons become small if they carry a large energy fraction z_h . According to the Lund model the prehadronic final state interactions therefore dominate the attenuation of high energy hadrons in DIS of nuclei.

For comparison Fig. 5 also shows the simple time estimates of Ref. (15) that

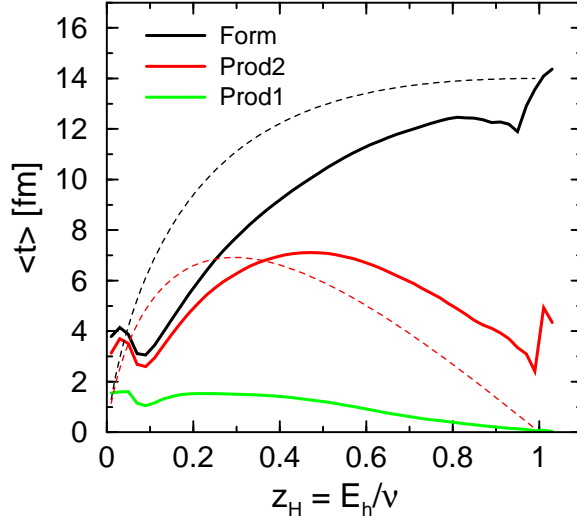


Fig. 5. The solid curves show the average production and formation times of hadrons in certain bins of the fractional hadron energy $z_h = E_h/\nu$. The kinematics are the same as for Fig. 3 ($\nu = 14 \text{ GeV}$, $Q^2 = 2.5 \text{ GeV}^2$). The dashed curves represent the results of the analytic estimate derived in Ref. (15) for the decay of an one-dimensional string into infinitely many fragments.

were derived analytically for the fragmentation of an one-dimensional string into infinitely many fragments. Obviously, the analytic estimates yield only a rough approximation of the average production and formation times in JETSET. Furthermore, it is not enough to know the average production and formation times if one wants to perform realistic calculations of nuclear reactions. Our method allows for a complete event-by-event simulation assigning the production and formation points and times to all hadrons in each JETSET event.

The distribution of production and formation points for pp -collisions at RHIC ($\sqrt{s} = 200 \text{ GeV}$) shown in Fig. 6 can be easily understood: Around the interaction point – corresponding to mid-rapidity – one has the broadest transverse momentum distribution and hence the largest transverse coordinates of the production and formation points. The regions with rapidity $y \rightarrow \infty$ mainly consist of remnants, that lead to hadron production along the beam axis. Since the rate of particles $dN/dp_\perp dy$ decreases approximately exponentially with increasing p_\perp , also the distribution of production and formation points in transversal direction does. (This is in contrast to the HERMES regime, where the photon sets an upper limit on the energy of the particles. Here this upper limit far out of reach and the transverse distribution is practically unconstrained.)

Of major experimental interest are high p_\perp -hadrons (e.g. $p_\perp > 4 \text{ GeV}$) at mid-rapidity ($|y| < 0.5$). The production and formation points applying these cuts are shown in Fig. 7. While the distribution of formation points supports the popular belief that high- p_\perp mid-rapidity hadrons at RHIC are produced

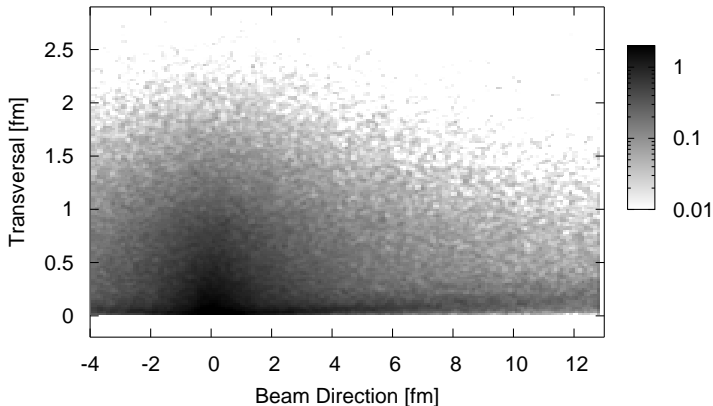


Fig. 6. *Production points for RHIC: $N + N @ \sqrt{s} = 200$ GeV. The picture is symmetric in horizontal direction, the contribution extends up to ± 100 fm.*

outside any fireball or deconfined phase, the distribution of production points tells another story: Most of the production points are within a transversal distance below 2 fm. However, we point out that the high hadron densities created in ultra-relativistic heavy ion collisions might strongly influence the string fragmentation process and that in the presence of a deconfined phase (QGP) the whole concept of hadronic strings becomes meaningless. For heavy ion collisions the presented production times and lengths should therefore be rather seen as lower estimates.

In order to quantify the findings from above, Tab. 1 presents the average proper times $\langle \tau \rangle$ of the production and formation vertices as well as the average production and formation times $\langle t \rangle$ in the laboratory frame. For comparison we also list the average values of the fraction t/τ and the Lorentz boost factor $\gamma = E_h/m_h$ of the considered hadron. Note that for each hadron there exist two production (proper-)times $(\tau_1) t_1$ and $(\tau_2) t_2$ – corresponding to the production of the first and second hadron constituent – as well as one yoyo-formation (proper-)time $(\tau_F) t_F$. The larger of the two production times t_2 is also called prehadron production time (4; 5).

The average production and formation *proper times* at HERMES seem to be almost independent of the particle species. On the other hand, one observes the same universal feature for the average *laboratory times* at RHIC conditions (with the implemented cuts). Furthermore, the ratio $\langle t/\tau \rangle$ deviates from the Lorentz factor $\langle \gamma \rangle$ of the corresponding hadron. Hence, the times that we have extracted from JETSET are in contradiction to the widely-used assumption that the hadron production and formation times in the lab frame are simply given as a product of the Lorentz-boost factor γ and an universal constant proper time.

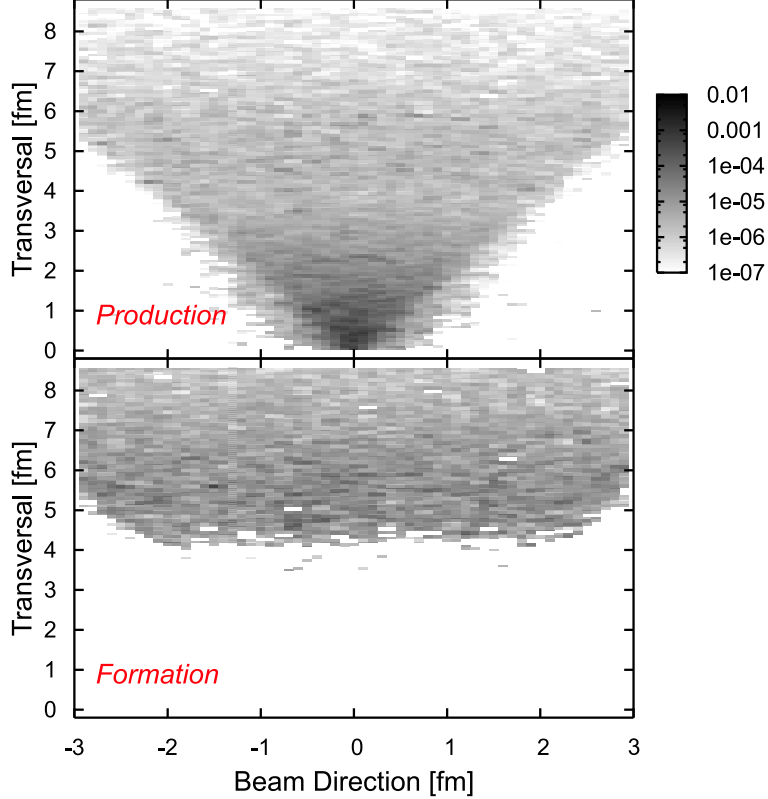


Fig. 7. *Production and formation points for RHIC($N + N @ \sqrt{s} = 200$ GeV) for mid-rapidity ($|y| < 0.5$) and high p_{\perp} : $p_{\perp} > 4$ GeV.*

In the presented work we have extracted the production and formation vertices of hadrons from the Lund fragmentation as modeled by JETSET. In contrast to other approaches, such as analytic derivations, we are able to extract the full four-dimensional information for each hadron produced in the fragmentation of a (gluonic) string on an event-by-event basis. For the first time we have presented quantitative results for realistic photon-nucleon reactions at HERMES energies and pp -collisions at RHIC using the Monte Carlo generator PYTHIA. However, we stress that our method can also be used for all other kinds of event generators which are based on JETSET for the fragmentation. We find that a large fraction of production and formation points at HERMES energies lie inside typical nuclear radii which underlines the importance of (pre-) hadronic FSI. Also the production points of high- p_{\perp} mid-rapidity hadrons at RHIC seem to lie inside the fireball region. Furthermore, we conclude that the conventional determination of hadron production and formation times by simply multiplying a (universal) constant proper time with the corresponding γ factor leads to misleading estimates for the hadron production and formation points.

This work is thought to be a 'proof of concept'. Detailed transport-theoretical studies of nuclear reactions (5; 9) that explicitly model the (pre-)hadronic FSI in the nuclear environment will follow. We point out that any event-by-event

| | $\langle\tau_1\rangle$ | $\langle\tau_2\rangle$ | $\langle\tau_F\rangle$ | $\langle t_1\rangle$ | $\langle t_2\rangle$ | $\langle t_F\rangle$ | $\langle\frac{t_1}{\tau_1}\rangle$ | $\langle\frac{t_2}{\tau_2}\rangle$ | $\langle\frac{t_F}{\tau_F}\rangle$ | $\langle\gamma\rangle$ |
|---|------------------------|------------------------|------------------------|----------------------|----------------------|----------------------|------------------------------------|------------------------------------|------------------------------------|------------------------|
| | fm | fm | fm | fm | fm | fm | | | | |
| HERMES: $W = 5 \text{ GeV}$, $Q^2 = 2.5 \text{ GeV}^2$ | | | | | | | | | | |
| π | 0.24 | 0.81 | 0.92 | 0.83 | 3.49 | 4.37 | 3.8 | 5.3 | 6.2 | 13.53 |
| ρ | 0.21 | 0.95 | 1.27 | 0.74 | 3.28 | 4.76 | 3.9 | 3.6 | 4.0 | 5.60 |
| N | 0.18 | 0.74 | 1.11 | 0.42 | 1.62 | 2.11 | 2.5 | 2.2 | 1.8 | 2.04 |
| RHIC: $ y < 0.5$, $p_\perp > 4 \text{ GeV}$ | | | | | | | | | | |
| π | 0.36 | 0.81 | 1.03 | 2.34 | 8.19 | 10.30 | 7.1 | 13.8 | 18.7 | 51.04 |
| ρ | 0.38 | 0.99 | 1.42 | 2.28 | 6.62 | 10.87 | 7.0 | 6.9 | 8.5 | 9.31 |
| N | 0.62 | 1.33 | 1.82 | 3.10 | 7.55 | 10.61 | 5.7 | 6.0 | 6.4 | 7.12 |

Table 1

Average production and formation times for pions, ρ mesons and baryons within specified kinematics (“HERMES”, “RHIC”). Proper times are labeled by τ , while t represents the corresponding time in the laboratory frame. γ is the relativistic boost factor of the hadron.

simulation based on our findings can account for all sorts of experimental cuts and detector efficiencies. Such models can therefore be directly compared with experimental data or used for detector simulations. They will help to clarify to what extend the experimentally observed hadron attenuation in nuclear DIS and ultra-relativistic heavy ion collisions is caused by the rescattering of the produced colorneutral (pre-)hadrons after fragmentation and what is caused by additional in-medium phenomena like a modification of the fragmentation function, a partonic energy loss or recombination effects.

This work has been supported by BMBF.

References

- [1] Y. Dokshitzer, V. Khoze, A. Mueller, S. Troyan, in: *Basics of perturbative QCD*, Editions Frontiers (1991).
- [2] A. Airapetian, et al., HERMES collaboration, Phys. Lett. B557 (2003) 37-46.
- [3] A. Accardi, V. Muccifora, H.-J. Pirner, Nucl. Phys. A720 (2003) 131-156.
- [4] B. Z. Kopeliovich, J. Nemchik, E. Predazzi, A. Hayashigaki, Nucl. Phys. A740 (2004) 211-245.
- [5] T. Falter, W. Cassing, K. Gallmeister, U. Mosel, Phys. Lett. B594 (2004) 61-68; Phys. Rev. C70 (2004) 054609.
- [6] Thomas Falter, Ph.D. Thesis, 2004, University of Giessen.

- [7] E. Wang, X.-N. Wang, Phys. Rev. Lett. 89 (2002) 162301; F. Arleo, Eur. Phys. J. C30 (2003) 213-221.
- [8] K. Gallmeister, C. Greiner, Z. Xu, Phys. Rev. C67 (2003) 044905.
- [9] W. Cassing, K. Gallmeister, C. Greiner, Nucl. Phys. A735 (2004) 277-299.
- [10] T. Sjöstrand, P. Eden, C. Friberg, L. Lönnblad, G. Miu, S. Mrenna, E. Norrbin, Comp. Phys. Commun. 135 (2001) 238; T. Sjöstrand, L. Lönnblad and S. Mrenna, LU TP 01-21 [hep-ph/0108264].
- [11] Patricia Liebing, Ph.D. Thesis, 2004, University of Hamburg.
- [12] B. Andersson, G. Gustafson, G. Ingelman, T. Sjöstrand, Phys. Rept. 97 (1983) 31; B. Anderson, in: *The Lund Model*, Cambridge University Press (1998).
- [13] Hong Pi, Comput. Phys. Commun. 71 (1992) 173; B. Andersson, G. Gustafson, Hong Pi, Z. Phys. C 57 (1993) 485.
- [14] T. Sjöstrand, Nucl. Phys. B248 (1984) 469.
- [15] A. Bialas, M. Gyulassy, Nucl. Phys. B291 (1987) 793.
- [16] P. Eden, JHEP 0005 (2000) 029.
- [17] A. Accardi, D. Grunewald, V. Muccifora and H. J. Pirner, hep-ph/0502072.